

# Toroidal Optical Dipole Traps for Atomic Bose-Einstein Condensates using Laguerre-Gaussian Beams

E. M. Wright, \* J. Arlt, and K. Dholakia

School of Physics & Astronomy

University of St. Andrews, North Haugh

St. Andrews, Fife KY16 9SS Scotland, UK

(December 2, 2024)

## Abstract

We theoretically investigate the use of red-detuned Laguerre-Gaussian (LG) laser beams of varying azimuthal mode index for producing toroidal optical dipole traps in two-dimensional atomic Bose-Einstein condensates. Higher-order LG beams provide deeper potential wells and tighter confinement for a fixed toroid radius and laser power. Numerical simulations of the loading of the toroidal trap from a variety of initial conditions is also given.

Typeset using REVTeX

---

\* Permanent address: Optical Sciences Center, University of Arizona, Tucson, AZ 85721, USA

## I. INTRODUCTION

Recent work has seen unprecedented advances in the preparation of Bose-Einstein condensates (BEC) of dilute alkali vapors [1–3]. These quantum degenerate systems have paved the way for numerous innovative studies of weakly interacting Bose gases. An important area within this field is the generation and study of quantized vortices on atomic mesoscopic rings and the potential to study effects due to persistent currents and Josephson effects [4–10]. Central to such studies is investigation of geometries for generation of a BEC in a toroidal trap [11]. Typically BEC is created in a magnetic trap that confines atoms in weak-field seeking states and is thus dependent on the atomic hyperfine states. A toroidal trap can then be formed by piercing a magnetic trap with a blue-detuned laser at its center [2]. However, the state dependence of the trapping is a limitation for advanced studies including multi-component spinor condensates. Further, the magnetic field is primarily dictated by the trapping requirements setting limitations on its spatial form and amplitude. Optical dipole traps can potentially circumvent these problems being state independent [12]. Importantly, the spatial form of the optical trap is dictated by the light beams used. This allows one to potentially generate arbitrary shapes of condensate [13]. Experimental work has shown the ability to transfer a condensate from a magnetic trap to an optical dipole trap created from a tightly focused Gaussian light beam [12].

The circularly symmetric Laguerre-Gaussian (LG) laser modes have generated substantial interest in recent years. This stems from the identification that they possess an orbital angular momentum of  $\ell\hbar$  per photon [14]. This is in addition to the spin angular momentum associated with the polarization state of the beam. The azimuthal index  $\ell$  refers to the number of  $2\pi$  phase cycles around the mode circumference. A given mode has  $p + 1$  radial nodes in the mode profile where  $p$  is the other index used in the LG mode description. One finds that LG beams with radial index  $p = 0$  are in the form of an annulus [15]. There are several techniques for production of LG modes including the use of a cylindrical lens mode converter [16] and holographic methods [17]. The latter technique allows generation of LG

modes from the fundamental output of a laser beam. The annulus becomes thinner as one increases the azimuthal index  $\ell$  of the mode [15].

In this work we present a technique for generating a toroidal BEC employing a Laguerre-Gaussian light beam. Single-ringed forms of such beams offer for the first time a direct possibility of generating ring-shaped condensates in an optical potential. We study the operation of this dipole trap as a function of azimuthal mode index and discuss the loading of condensates into such optical traps from a variety of initial conditions.

## II. BASIC MODEL AND EQUATIONS

### A. Gross-Pitaevskii equation

The basic model we consider is shown in Fig. 1 and comprises a two-dimensional (2D) BEC whose normalized mode profile is frozen by tight confinement along the  $z$ -direction, and which is placed at the focus of an off-resonant LG laser beam of frequency  $\omega_L$  incident along the  $z$ -axis that provides a two-dimensional optical potential [12]. The tight confinement may be provided, for example, by an independent sheet potential using a scanned optical dipole potential [13]. Then the Gross-Pitaevskii equation (GPE) describing the macroscopic wavefunction  $\psi(\mathbf{r}_\perp, t)$  for the quasi-2D motion can be written as [18,19]

$$i\hbar \frac{\partial \psi}{\partial t} = -\frac{\hbar^2}{2M} \nabla_\perp^2 \psi + U(\mathbf{r}_\perp) \psi + gN|\psi|^2\psi, \quad (1)$$

where  $\mathbf{r}_\perp$  is the two-dimensional position vector in the plane perpendicular to  $z$ ,  $\nabla_\perp^2$  the corresponding two-dimensional Laplacian,  $M$  is the atomic mass, and  $g$  is the effective short-range interaction strength. The potential term on the right-hand-side

$$U(\mathbf{r}_\perp) = \frac{\hbar\Gamma^2}{8\Delta} \left( \frac{I(\mathbf{r}_\perp)}{I_{\text{Sat}}} \right) \quad (2)$$

describes the 2D optical dipole potential with  $\Delta = \omega_L - \omega_A$  the laser detuning from the optical transition frequency  $\omega_A$ ,  $\Gamma$  the natural linewidth of the optical transition,  $I_{\text{Sat}}$  is the resonant saturation intensity, and  $I(\mathbf{r}_\perp) = \frac{1}{2}\epsilon_0 cn|E(\mathbf{r}_\perp, 0)|^2$ , assuming the BEC is centered

at  $z = 0$  and has a thickness less than the Rayleigh range of the focused beam. In addition, we assume that the intensity profile of the LG beam is undistorted upon propagation through the 2D BEC, which is reasonable for a thin BEC. We remark, however, that the LG beam becomes spatially phase-modulated upon transiting the BEC, resulting in a changed far field profile of the beam that could prove a useful diagnostic of the BEC density profile.

For later purposes we point out the GPE conserves both the wave function norm

$$n(t) = \int d^2\mathbf{r}_\perp |\psi(\mathbf{r}_\perp, t)|^2, \quad (3)$$

and also the effective single-particle Hamiltonian

$$H(t) = \int d^2\mathbf{r}_\perp \left[ \frac{\hbar^2}{2M} |\nabla\psi|^2 + U(\mathbf{r}_\perp) |\psi|^2 + \frac{gN}{2} |\psi|^4 \right]. \quad (4)$$

## B. Toroidal optical dipole potential

Our goal in this work is to explore theoretically the use of LG beams for producing toroidal optical dipole traps, the dipole potential being proportional to the laser intensity in the limit of large detunings considered here. The intensity profile of an LG beam at its focus ( $z = 0$ ) in cylindrical coordinates ( $\mathbf{r}_\perp = (r, \theta)$ ) takes the form

$$I_{p,\ell}(r) = \frac{2p!}{(p + |\ell|)!} \frac{P_0}{\pi w_{p,\ell}^2} \left( \frac{2r^2}{w_{p,\ell}^2} \right)^{|\ell|} e^{-2r^2/w_{p,\ell}^2} \left[ L_p^{|\ell|} \left( \frac{2r^2}{w_{p,\ell}^2} \right) \right]^2, \quad (5)$$

where  $P_0$  is the beam power,  $\ell$  is the azimuthal mode index, the field having a variation  $\exp(i\ell\theta)$ ,  $p$  is the radial mode index which is the number of radial intensity maxima,  $w_{p,\ell}$  is the mode spot size, and  $L_p^{|\ell|}$  is a generalized Laguerre polynomial. Here we create a single-ringed toroidal trap using a red-detuned laser field ( $\Delta < 0$ ), so the atoms are light-seeking, using an LG beam with  $p = 0$ , in which case  $L_0^{|\ell|} = 1$ , and we hereafter drop the  $p$  index and take  $\ell > 0$ . Then for each value of  $\ell$  the intensity profile has a single maximum at  $r_\ell = w_\ell \sqrt{\frac{\ell}{2}}$  [20]. Thus, in order to produce a toroid of a fixed radius  $r_\ell = r_T$ , we need to choose the spot size  $w_\ell$  for each azimuthal mode such that

$$w_\ell = r_T \sqrt{\frac{2}{\ell}}. \quad (6)$$

Furthermore, for a given  $\ell$  the peak intensity at the toroid center  $r = r_T$  may be written as

$$I_\ell = \frac{2P_0}{\pi w_\ell^2} \left( \frac{\ell^\ell e^{-\ell}}{\ell!} \right) = I_1 \left( \frac{\ell^{\ell+1} e^{-(\ell-1)}}{\ell!} \right) \approx I_1 \sqrt{\ell}, \quad (7)$$

with  $I_1 = e^{-1} P_0 / \pi r_T^2$  the peak intensity for  $\ell = 1$  [20]. Here in the expression for  $I_\ell$  we have used Stirling's formula  $\ell! \approx \sqrt{2\pi\ell} \cdot \ell^\ell / e^\ell$ , and we see that the peak intensity scales as  $\sqrt{\ell}$ .

Gathering the above results together, for a fixed laser power  $P_0$  we may write the optical dipole potential (eq. (2)) in the following form which is useful for comparison between different values of  $\ell$

$$U_\ell(r) = U_\ell \left( \frac{r}{r_T} \right)^{2\ell} e^{-\ell(r^2/r_T^2 - 1)}, \quad (8)$$

where

$$U_1 = \frac{\hbar\Gamma^2}{8\Delta} \left( \frac{e^{-1} P_0}{\pi r_T^2 I_{\text{Sat}}} \right), \quad U_\ell = U_1 \left( \frac{\ell^{\ell+1} e^{-(\ell-1)}}{\ell!} \right) \approx U_1 \sqrt{\ell}, \quad (9)$$

$U_1$  being the optical dipole potential well depth for  $\ell = 1$  at the toroid radius  $r_T$ . Figure 2 shows the normalized optical dipole potential  $U_\ell(r)/|U_1|$  versus  $r/r_T$  for various azimuthal mode indices  $\ell$ , a red-detuned laser, and fixed laser power and toroid radius, i.e. fixed  $U_1$ . Here we see that as  $\ell$  increases the toroidal trap becomes deeper and tighter, meaning that higher-order LG beams present advantages for making tight toroidal dipole traps.

### III. GROUND STATE TOROIDAL SOLUTIONS

In this section we elucidate the ground state properties of toroidal traps using the harmonic oscillator and Thomas-Fermi approximations. These approximate solutions amply illustrate the key features of the problem.

### A. Thomas-Fermi solution

Setting  $\psi(r, \theta, t) = \phi(r) \exp(-i\mu t/\hbar)$  for the cylindrically symmetric ground state we obtain

$$\mu\phi = -\frac{\hbar^2}{2M}\nabla_{\perp}^2\phi + U_{\ell}(r)\phi + gN|\phi|^2\phi, \quad (10)$$

with  $\mu$  the chemical potential. To obtain insight into the solutions of this equation we consider the harmonic oscillator approximation to the toroidal dipole potential (eq. (8)) trap around  $r = r_T$ ,

$$U_{\ell}(r_T + \delta r) \approx U_{\ell} \left( 1 - 2\ell \frac{\delta r^2}{r_T^2} + \dots \right). \quad (11)$$

If we furthermore employ the Thomas-Fermi approximation [21,22], in which the kinetic energy term is neglected in comparison to the mean field energy, then we obtain the approximate GPE

$$(\mu - U_{\ell})\phi \approx \frac{1}{2}M\Omega_{\ell}^2\delta r^2\phi + gN|\phi|^2\phi \quad (12)$$

where the effective harmonic oscillator frequencies are

$$\Omega_{\ell} = 2\sqrt{\frac{|U_1|}{Mr_T^2}} \left( \frac{\ell^{\ell+2}e^{-(\ell-1)}}{\ell!} \right)^{1/2} \approx 2\sqrt{\frac{|U_1|}{Mr_T^2}} \cdot \ell^{3/4}, \quad (13)$$

where Stirling's formula was used in the last expression. Equation (12) has the approximate ring solution ( $r_T - \Delta r_{\ell} \leq r \leq r_T + \Delta r_{\ell}$ )

$$\mu = U_{\ell} + \frac{gN}{2\pi r_T \Delta r_{\ell}}, \quad |\phi(r)|^2 = \frac{1}{2\pi r_T \Delta r_{\ell}} \left( 1 - \frac{(r - r_T)^2}{\Delta r_{\ell}^2} \right), \quad (14)$$

where the ring width is given by

$$\left( \frac{\Delta r_{\ell}}{r_T} \right) = \left( \frac{gN}{4\pi|U_1|r_T^2} \right)^{1/3} \left( \frac{\ell!}{\ell^{\ell+2}e^{-(\ell-1)}} \right)^{1/3} \approx \left( \frac{gN}{4\pi|U_1|r_T^2} \right)^{1/3} \ell^{-1/2}. \quad (15)$$

These solutions correspond to ring-shaped BEC density profiles which are peaked at  $r = r_T$  and have a width  $2\Delta r_{\ell}$ . We see that as the azimuthal mode index  $\ell$  is increased with all other

parameters fixed the radial harmonic oscillator frequency increases  $\Omega_\ell \propto \ell^{3/4}$ , and the ring width decreases  $\Delta r_\ell \propto \ell^{-1/2}$ . Thus, using higher-order LG beams provides an advantage for making tight bound toroidal rings as commented earlier.

The 2D Thomas-Fermi solution above should be applicable under the combined conditions  $gN \gg \hbar^2/2M$  and  $\Delta r_\ell/r_T \ll 1$ , which ensure that the mean-field energy is greater than the kinetic energy, and the ring width is less than the toroid radius. The latter condition is also required for the validity of the harmonic oscillator approximation.

## B. Scaling

To explore the parameter space for the toroidal trap it is useful to introduce appropriately scaled units. For a trap of radius  $r_T$  we scale all lengths as  $\rho_\perp = \mathbf{r}_\perp/r_T$ , all energies are scaled to  $\hbar\omega_T = \hbar^2/Mr_T^2$ , and we introduce a dimensionless time  $\tau = \omega_T t$ . In these units the GPE becomes

$$i\frac{\partial\varphi}{\partial\tau} = -\frac{1}{2}\nabla_\perp^2\varphi + u_\ell(\rho)\varphi + \pi\eta N|\varphi|^2\varphi, \quad (16)$$

where  $\varphi = r_T\psi$ ,  $u_\ell = U_\ell/\hbar\omega_T$ , and  $\eta = Mg/\pi\hbar^2$  is a dimensionless measure of the repulsive many-body interactions [18,19,23]. We shall use the above scaled GPE in our numerical simulations of loading toroidal optical dipole traps.

Turning to the Thomas-Fermi solution, in dimensionless units the radial harmonic oscillator frequency and the ring width become

$$\frac{\Omega_\ell}{\omega_T} \approx 2\sqrt{|u_1|} \cdot \ell^{3/4} \quad \frac{\Delta r_\ell}{r_T} \approx \left(\frac{\eta N}{4|u_1|}\right)^{1/3} \ell^{-1/2} \quad (17)$$

and the chemical potential is given by

$$\frac{\mu}{\hbar\omega_T} \approx u_1\ell^{1/2} \left[ 1 + 2 \cdot \text{sgn}(u_1) \left(\frac{\eta N}{4|u_1|}\right)^{2/3} \right] \quad (18)$$

where Stirling's formula has been used. These solutions depend on the dimensionless well depth  $u_1$  for  $\ell = 1$  which is given explicitly by

$$u_1 = \frac{U_1}{\hbar\omega_T} = \frac{\Gamma^2}{8\hbar\Delta} \left( \frac{e^{-1}MP_0}{\pi I_{\text{Sat}}} \right), \quad (19)$$

and is independent of the toroid radius.

In dimensionless form the condition  $gN \gg \hbar^2/2M$  for applicability of the Thomas-Fermi approximation becomes  $\eta N \gg 1/(2\pi)$ . Combining this with the condition  $\Delta r_\ell/r_T < 1$  yields the constraint on the number of particles

$$\frac{1}{2\pi} < \eta N < 4|u_1|\sqrt{\ell}, \quad (20)$$

which shows that traps using higher azimuthal mode index can hold more atoms, all other parameters being equal.

### C. Parameter values

To illustrate the basic scales involved in toroidal traps we consider the case of the  $\lambda_A = 589$  nm transition of Na using a laser wavelength of  $\lambda_L = 985$  nm and a toroid radius of  $r_T = 10 \mu\text{m}$ , these values being used throughout this paper. Then using the parameter values  $I_{\text{Sat}} = 63 \text{ W/m}^2$ ,  $\Gamma = 2\pi \times 9.89 \text{ MHz}$ , we obtain  $u_\ell = u_1\sqrt{\ell} = -253 \times P_0\sqrt{\ell}$ , with  $P_0$  in milli-Watts. Using  $\hbar\omega_T \equiv 2.1 \times 10^{-10} \text{ K}$ , with corresponding time scale  $1/\omega_T = 36 \text{ ms}$ , for a given azimuthal mode index  $\ell$  this potential depth translates to  $u_\ell \equiv 53 \times P_0\sqrt{\ell} \text{ nK}$ . The corresponding effective oscillator frequencies in the toroidal trap are then  $\Omega_\ell = 2\pi \times 0.14P_0^{1/2}\ell^{3/4} \text{ kHz}$ . Consider therefore the case of  $P_0 = 1 \text{ mW}$  so that  $u_1 = -253$ . For two-dimensional BECs a characteristic value for the many-body parameter is  $\eta \approx 10^{-3}$  [19,23]. Then for  $N = 10^5$  and  $\ell = 6$  we have  $\Delta r_6 = 1.9 \mu\text{m}$ , and  $\Omega_6 = 2\pi \times 0.54 \text{ kHz}$ . This is not a particularly tight ring but tighter confinement can be achieved by increasing the azimuthal mode index. Figure 3 shows the variation of the oscillator frequency  $\Omega_\ell/2\pi$  in kHz (solid line), and  $\Delta r_\ell$  in microns (dashed line) both versus  $\ell$  for  $u_1 = -253$ ,  $\eta N = 100$ , and displays the advantage of using high azimuthal mode index. We note that it is difficult to produce LG modes with very high azimuthal index ( $\ell > 6$ ) due to decreasing mode purity from holographic generation. However, other techniques exist for generating narrow annular

beams, e.g. using an axicon [24]. Typically the radial spread of such beams is very small, thus they would allow one to explore the region of tight radial confinement seen for LG beams with  $\ell \geq 20$  (see Fig. 3).

#### IV. LOADING A TOROIDAL OPTICAL DIPOLE TRAP

Having established that LG beams can provide toroidal traps for 2D BECs the issue arises of how to load atoms into the ground state of the trap. It does not seem feasible to condense directly in the toroidal trap as it does not lend itself to evaporative cooling and the laser field could lead to heating. The solution is then to load into the toroidal trap from an existing BEC, e.g. a magnetic trap or sheet dipole potential trap [13]. Here we consider loading of a toroidal trap from an initial 2D ring BEC, for example using a magnetic trap with a blue-detuned laser piercing its center [2], and also from a centrally peaked BEC as is the case for conventional harmonic traps. The calculations presented here demonstrate that it is in principle possible to load toroidal traps and we use illustrative examples which highlight the issues involved.

##### A. Types of initial condition

We have numerically solved the GPE (16) for a variety of initial conditions with the exact optical dipole potential in Eq. (8). We consider the situation that for  $t < 0$  the BEC is in the ground state of a prescribed potential which is turned off for  $t > 0$  and the toroidal LG trap is turned on. To model this situation we have considered a variety of initial conditions at  $t = 0$  and their subsequent evolution. Rather than dwelling on a specific potential model for  $t < 0$  we consider the super-Gaussian initial macroscopic wave functions

$$\psi(r, 0) = \mathcal{N} e^{-(r-r_{\text{peak}})^m/w^m}, \quad (21)$$

where  $\mathcal{N}$  is a normalization constant,  $w$  is the width of the initial wave function,  $m \geq 2$  is the order of the super-Gaussian,  $m = 2$  being the usual Gaussian, and  $r_{\text{peak}}$  is the displacement

of the density peak away from the origin: for  $r_{\text{peak}} = 0$  we have a centrally peaked initial density,  $r_{\text{peak}} = r_T$  gives an initial ring BEC with its peak at the toroid radius. As  $m$  increases the initial condition becomes more top-hat like, representative of the broadening due to repulsive many-body effects. For the numerics presented here we set  $m = 8$ .

We have numerically solved the GPE (16) for a variety of initial conditions with the exact optical dipole potential in Eq. (8) subject to the above initial conditions using the split-step beam propagation method [25]. In implementing this scheme we have included absorbing boundary conditions at the edge of the numerical grid, thereby simulating losses due to radially outward going atoms. We tested that the numerical results presented were not sensitive to the placement of the absorber. Thus, in our simulations the norm  $n(t)$  in Eq. (3) of the macroscopic wave function is not conserved at unity. However, the norm  $n(t) \leq 1$  is actually a measure of the fraction of initial atoms that are captured in the toroidal trap.

For most of the simulations presented we chose  $\ell = 6$  as this is characteristic of the LG beams that can be generated reliably experimentally at present [15].

### B. Initial ring BEC

First we will discuss the loading of the toroidal optical dipole trap with a BEC that is already ring shaped. Although the BEC has already the desired shape, this transfer from a magnetic-based ring trap to a toroidal trap is still of importance as this trap can confine multi-component condensates in different Zeeman sublevels. For an initial ring BEC the ground state of the toroidal trap can be excited by reasonably matching the initial and ground state wave functions. Figure 4 shows two examples of the computed dynamics for an initial ring BEC formed in Na with  $u_1 = -25.3$  ( $P_0 = 0.1$  mW), and  $\eta N = 50$ . For these parameters and  $\ell = 6$  the Thomas-Fermi theory of the last section gives a ring width of  $\Delta r_6 = 3.2 \mu\text{m}$ . In Fig. 4(a), which shows a gray-scale plot of the 2D atomic density  $|\varphi(x, 0, t)|^2$  versus time in ms along the horizontal axis and radius  $x$  in microns along the vertical axis, we used  $\ell = 6$ ,  $w = 4 \mu\text{m}$ , and after a transient the density profile settles down

to a steady ring of smaller width than the input. The transient involves expansion of the atoms outward from the ring and also inwards towards the origin, and the peak at the origin seen for  $t \approx 3.2$  ms is due to interference between the inwardly propagating circular atomic waves. The outward propagating atomic waves leads to an effective loss mechanism which allows for the damping of the initial wave function towards the ground state toroidal BEC. The final ring contains  $n \approx 90\%$  of the initial atoms. Figure 4(b) shows a gray-scale plot of the 2D atomic density for the same parameters as 4(a) except  $\ell = 2$ , for which  $\Delta r_2 = 5.6\mu\text{m}$ , so that the input with  $w = 2.5\mu\text{m}$  is now half the expected ring width. After a considerably larger transient than in Fig. 4(a) the density again settles down but now to a larger ring than the input containing about  $n \approx 80\%$  of the initial atoms. Notice, however, that for  $t > 15$  ms the atomic density shows a further transient, and this is caused by weak atomic waves caught around the origin that start to leak out, as revealed by detailed examination of the data.

For these simulations we have used a rather low laser power  $P_0 = 0.1\text{ mW}$ , so that the toroidal trap depth is only about 13 nK for  $\ell = 6$ . For such low trap depths collisions with background gas and beam pointing fluctuations could present sources of heating and trap loss [26]. However, we have chosen such a loosely bound toroidal trap as an illustrative example of loading since tighter traps (larger  $|u_1|$ ) are generally easier to excite by suitably matched initial ring BECs as the ground state and next excited state have a larger energy separation. Thus the present example shows that there is considerable robustness in loading from initial ring BECs, as expected intuitively.

### C. Initial centrally peaked BEC

Figure 5 shows representative 2D atomic density plots from simulations of loading from an initial centrally peaked ( $r_{\text{peak}} = 0$ ) Na BEC with  $m = 8, u_1 = -100$  ( $P_0 = 0.40\text{ mW}$ ), the corresponding trap depth being  $21.2\sqrt{\ell}\text{nK}$ , and  $\eta N = 400$ . The plots are for different initial BEC widths (a)  $w = r_T = 10\mu\text{m}$  with  $\ell = 6$ , (b)  $w = 14\mu\text{m}$  with  $\ell = 6$ , and (c)  $w = 14\mu\text{m}$ ,

with  $\ell = 2$ . Case (a) shows very little signs of trapping in the toroid which is centered at  $r_T = 10 \mu\text{m}$ , but (b) with an increased BEC width of  $w = 14 \mu\text{m}$  now shows substantial trapping with  $N = 90\%$  of the initial atoms trapped. What distinguishes these two case is that the initial Hamiltonian in Eq. (4), which we evaluated numerically, is  $H(0)/\hbar\omega_T = 148$  in case (a) and  $H(0)/\hbar\omega_T = -16.6$  for case (b). The Hamiltonian has three contributions, the kinetic energy which is positive, the optical dipole potential which for a red-detuned laser is negative, and the nonlinear term due to many-body repulsion which is positive. As we simulate the effects of atom losses due to outward propagating atoms using the absorbing boundary, the atom number decreases and so typically does the Hamiltonian as the initial BEC evolves. Physically, as we consider red-detuned traps that have negative optical dipole potentials which go to zero away from the trap, atoms with energies above the trap energy of zero will tend to be lost from the toroidal trap. For case (a) the initial Hamiltonian or energy is above the trap energy and the atoms fly above the toroidal trap under the influence of the repulsive many-body effects. Indeed the initial density profile with  $w = 10 \mu\text{m}$  overlaps the toroidal trap very little, leaving only positive contributions to the Hamiltonian in Eq. (4). In contrast, for the wider initial BEC in Fig. 5(b) the initial density profile overlaps the toroidal trap giving a net Hamiltonian less than the trap energy, so trapping becomes possible. We remark that the requirement that the initial Hamiltonian be less than the trap energy is a necessary but not sufficient condition for trapping, as there is still dependence on the initial density profile. For example, Fig. 5(c) is the same as in 5(b) except  $u_1 = -253$  ( $P_0 = 1\text{mW}$ ), the corresponding trap depth being 130 nK for  $\ell = 6$ . In this case  $H(0)/\hbar\omega_T = -216$ , well below the trap energy, but Fig. 5(c) shows that the atoms do not cleanly load into the ground state of the toroidal trap, but rather the density displays undamped oscillations on the time scale of the simulation. This oscillatory behavior is typically a feature for deeper traps. We have begun to explore methods of smoothing the loading of deeper toroidal traps, such as tapering the turn-on of the optical potential and phase-imprinting the initial BEC so that it moves towards a ring. These methods do smooth the loading process and we shall report on these issues along with the effects of beam misalignments in a future publication.

## V. SUMMARY AND CONCLUSIONS

In this paper we have shown that Laguerre-Gaussian beams provide a flexible means for forming toroidal optical dipole traps in 2D atomic BECs, and that the toroidal traps can be loaded from initial conditions representative of conventional magnetic traps. It remains to be seen how tight the atoms can be confined in these rings, and detailed numerical studies are underway. This work is a first step towards developing toroidal traps which shall act as mesoscopic rings for atoms for a variety of basic and applied studies [4–10]. For example, once a BEC is prepared in its ground state of the toroidal trap a vortex state of variable angular momentum can be excited using Raman coupling (involving a second LG beam) to another Zeeman sublevel [27], hence allowing for studies of ring vortices and persistent currents on a torus [4,5,9]. Also, as our toroidal trap does not involve a magnetic trap it allows for studies of multi-component BECs trapped on a ring [10]. In the limit of small number of atoms there is also the possibility of realizing a Tonk’s gas of impenetrable bosons on a ring [28–30], which has been predicted to exhibit dark solitons [31]. Furthermore, by looking at higher-order LG modes with different radial index  $p$ , and hence multiple concentric rings, we can create coaxial toroidal traps for the BECs, hence allowing for radial tunneling between condensates. In particular, multiple rings could create a circular grating for atoms which could in principle act as the feedback mechanism for a 2D atom laser, by analogy to circular grating optical lasers [32]. On the applied side, once a ring BEC is formed we can further pierce it with blue-detuned lasers at positions along its perimeter to form tunnel-junctions akin to superconducting links. One can then envision a range of sensors, e.g. rotation, based on the sensitivity of the tunneling current to any perturbation of the system. In principle, large rings could be made by first loading a small ring and then adiabatically expanding the LG light mode incident on the BEC, hence very sensitive matter-wave sensors of inertial forces could result.

EMW was supported in part by the Office of Naval Research Contract No. N00014-99-1-

0806, and ARO. KD acknowledges the support of the UK Engineering and Physical Sciences Research Council.

## REFERENCES

- [1] M. H. Anderson, J. R. Ensher, M. R. Matthews, C. E. Wieman, and E. A. Cornell, *Science* **269**, 198 (1995).
- [2] K. B. Davis, M. O. Mewes, M. R. Andrews, N. J. van Druten, D. S. Durfee, D. M. Kurn, and W. Ketterle, *Phys. Rev. Lett.* **75**, 3969 (1995).
- [3] For a recent review of the field, see F. Dalfovo, S. Giorgini, L. P. Pitaevskii, and S. Stringari, *Rev. Mod. Phys.* **71**, 463 (1999).
- [4] D. S. Rokhsar, “Dilute Bose gas on a torus,” cond-mat/9709212 (1997).
- [5] J. Javanainen, S. M. Paik, and S. M. Yoo, *Phys. Rev. A* **58**, 580 (1998).
- [6] Th. Busch and J. R. Anglin, *Phys. Rev. A* **60**, R2669 (1999).
- [7] K. G. Petrosyan and L. You, *Phys. Rev. A* **59**, 639 (1999).
- [8] M. Benaki, S. Raghavan, A. Smerzi, S. Fantoni, and S. R. Shenoy, *Europhys. Lett.* **46**, 275 (1999).
- [9] Y. L-Geller, and P. M. Goldbart, *Phys. Rev. A* **6104**, 3609 (2000).
- [10] T. Isoshima, M. Nakahara, T. Ohmi and K. Machida, *Phys. Rev. A* **61**, 063610 (2000).
- [11] L. Salasnich, A. Parola, and L. Reatto, *Phys. Rev. A* **59**, 2990 (1999).
- [12] D. M. Stamper-Kurn, M. R. Andrews, A. P. Chikkatur, S. Inouye, H.-J. Meisner, J. Stenger, and W. Ketterle, *Phys. Rev. Lett.* **80**, 2027 (1998).
- [13] Dallin S. Durfee, Ph. D thesis, *Dynamic properties of dilute Bose-Einstein condensates*, (MIT, 1999).
- [14] L. Allen, M. W. Beijersbergen, R. J. C. Spreeuw, and J. P. Woerdman, *Phys. Rev. A* **45**, 8185 (1992).
- [15] M. A. Clifford, J. Arlt, J. Courtial, and K. Dholakia, *Opt. Commun.* **156** 300 (1998).

[16] M. W. Beijersbergen, L. Allen, H. E. L. O. Vervaeke, and J. P. Woerdman, *Opt. Commun.* **96** 123 (1993).

[17] H. He, N. R. Heckenberg, and H. Rubinsztein-Dunlop, *J. Mod. Opt.* **42**, 217 (1995).

[18] S.-H Kim, C. Won, S. D. Oh, and W. Jhe, “Bose-Einstein condensation in a two-dimensional trap,” cond-mat/0003342.

[19] D. S. Petrov, M. Holzmann, and G. V. Shlyapnikov, *Phys. Rev. Lett.* **84**, 2551 (2000).

[20] J. Arlt, T. Hitomi, and K. Dholakia, “Atom guiding along Laguerre-Gaussian and Bessel light beams,” published on-line *Appl. Phys. B* (2000).

[21] M. Edwards and K. Burnett, *Phys. Rev. A* **51**, 1382 (1995).

[22] G. Baym and C. J. Pethick, *Phys. Rev. Lett.* **76**, 6 (1996).

[23] M. Bayindir and B. Tanatar, *Phys. Rev. A* **58**, 3134 (1998).

[24] I. Manek, Y. B. Ovchinnikov, and R. Grimm, *Opt. Commun.* **147** 67 (1998).

[25] J. A. Fleck, J. R. Morris, and M. D. Feit, *Appl. Opt.* **10**, 129 (1976).

[26] T. A. Savard, K. M. O’Hara, and J. E. Thomas, *Phys. Rev. A* **56** R1095 (1997).

[27] K.-P Marzlin, W. Zhang, and E. M. Wright, *Phys. Rev. Lett.* **79**, 4728 (1997).

[28] L. Tonks, *Phys. Rev* **50**, 955 (1936).

[29] M. Olshanii, *Phys. Rev. Lett.* **81**, 938 (1998).

[30] D. S. Petrov, G. V. Shlyapnikov, and J. T. M. Walraven, “Regimes of quantum degeneracy in trapped 1D gases,” cond-mat/0006339 (2000).

[31] M. D. Girardeau and E. M. Wright, *Phys. Rev. Lett.* **84**, 5691 (2000).

[32] T. Erdogan and D. G. Hall, *J. Appl. Phys.* **68**, 1435 (1990).

## FIGURES

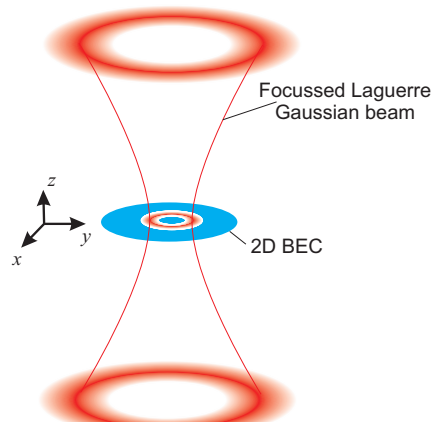
FIG. 1. Our basic model comprises a two-dimensional BEC which is illuminated by a red-detuned LG beam traveling along the  $z$ -axis and which acts as a toroidal trap.

FIG. 2. Normalized optical dipole potential  $U_\ell(r)/|U_1|$  versus  $r/r_T$  for various azimuthal mode indices  $\ell$  for fixed laser power and toroid radius. For the red-detuning assumed here, as  $\ell$  increases the toroidal trap becomes deeper and tighter.

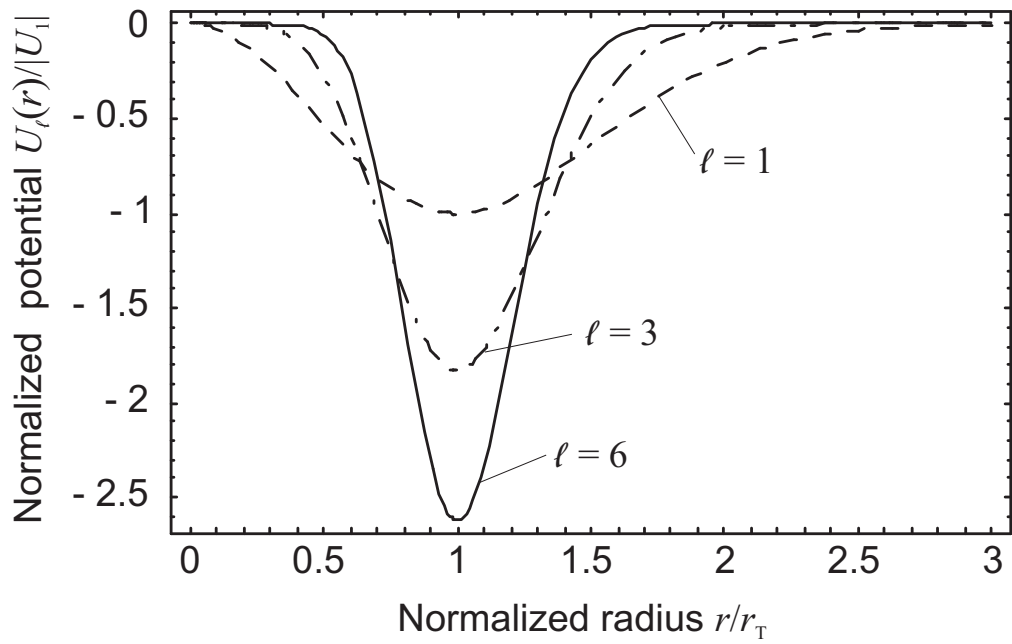
FIG. 3. Variation of the oscillator frequency  $\Omega_\ell/2\pi$  in kHz (solid line), and width  $\Delta r_\ell$  in microns (dashed line) both versus  $\ell$  for  $u_1 = -253$ ,  $\eta N = 100$ .

FIG. 4. Loading of a toroidal trap from an initial ring BEC with  $r_{\text{peak}} = 10 \mu\text{m}$  and  $m = 8$ : Gray scale plots of the evolution of the atomic density  $|\varphi|^2$  for  $u_1 = -25.3$ ,  $\eta N = 50$ , and (a)  $w = 4 \mu\text{m}$  with  $\ell = 6$ , (b)  $w = 4$  with  $\ell = 2$ .

FIG. 5. Loading of a toroidal trap from an initial super-Gaussian with  $m = 8$ : Gray scale plots of the evolution of the atomic density  $|\varphi|^2(x, 0, t)$  for  $u_1 = -100$ ,  $\eta N = 400$ ,  $\ell = 6$ , and (a)  $w = r_T = 10 \mu\text{m}$  with  $H(0)/\hbar\omega_T = 148$ , (b)  $w = 14 \mu\text{m}$  with  $H(0)/\hbar\omega_T = -16.6$ . (c) is for the same parameters as (b) except  $u_1 = -253$  giving  $H(0)/\hbar\omega_T = -216$ .



**Figure 1:** E. M. Wright *et al.*, Toroidal Optical Dipole Traps...



**Figure 2:** E. M. Wright *et al.*, Toroidal Optical Dipole Traps...

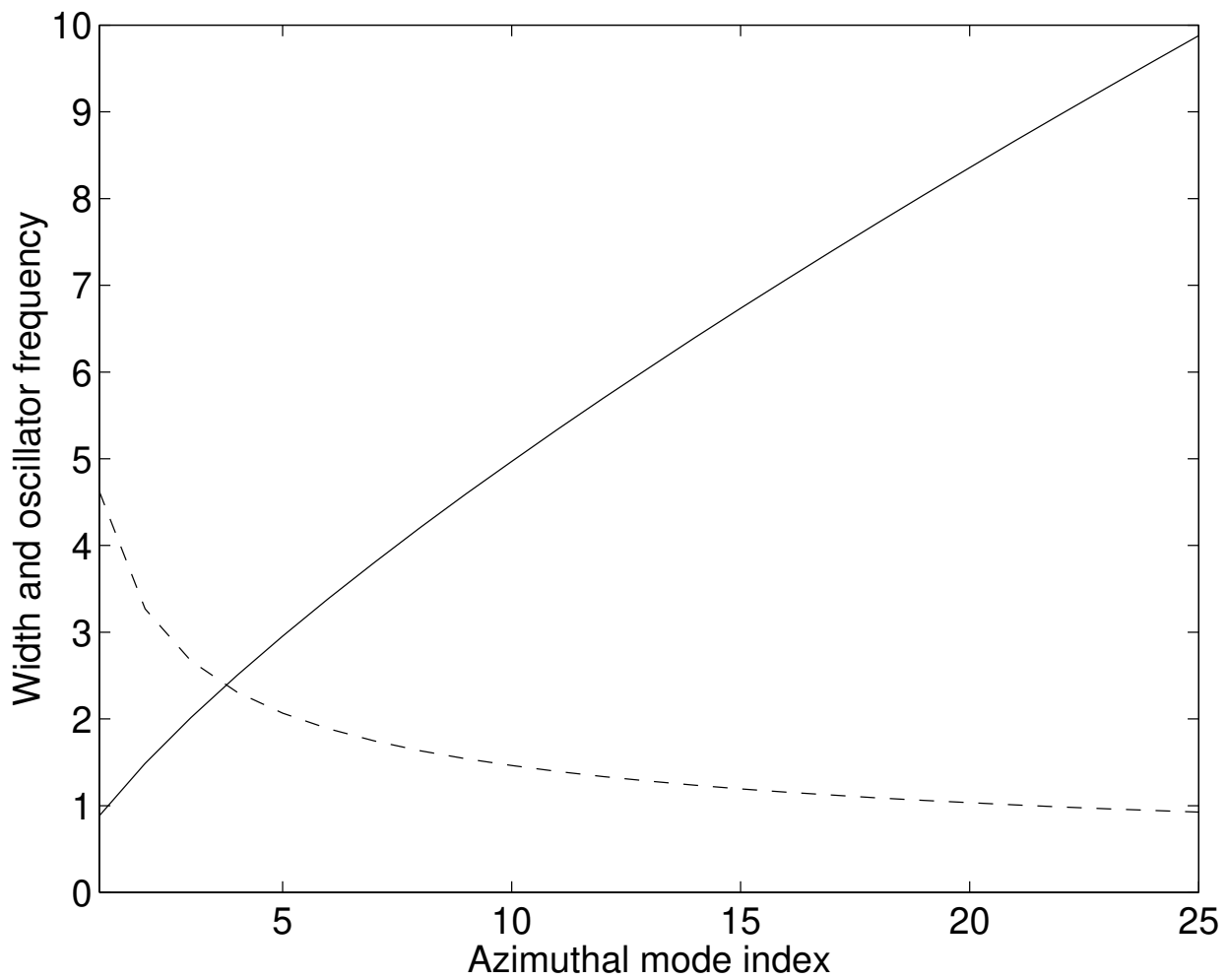


Figure 3

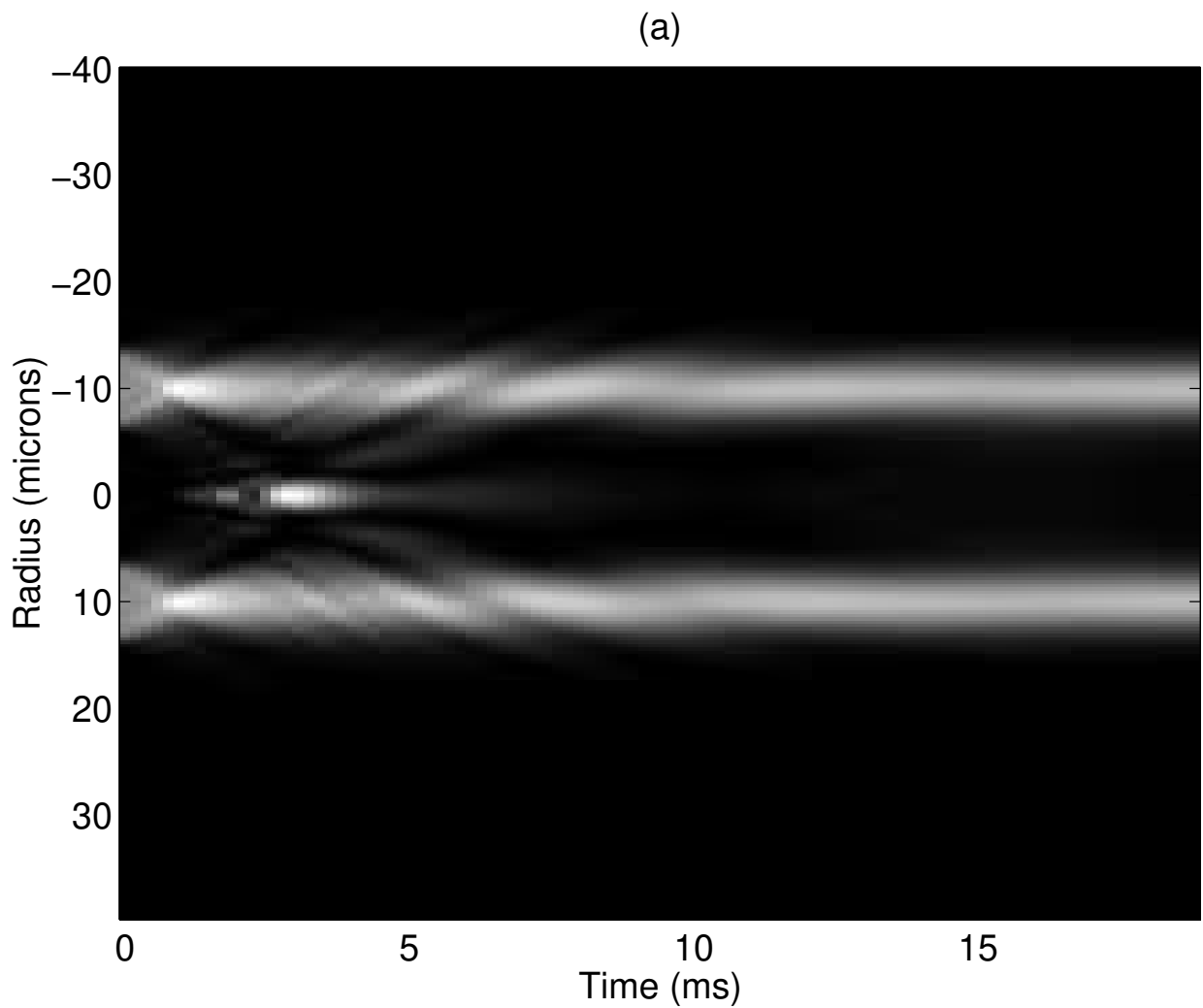


Figure 4(a)

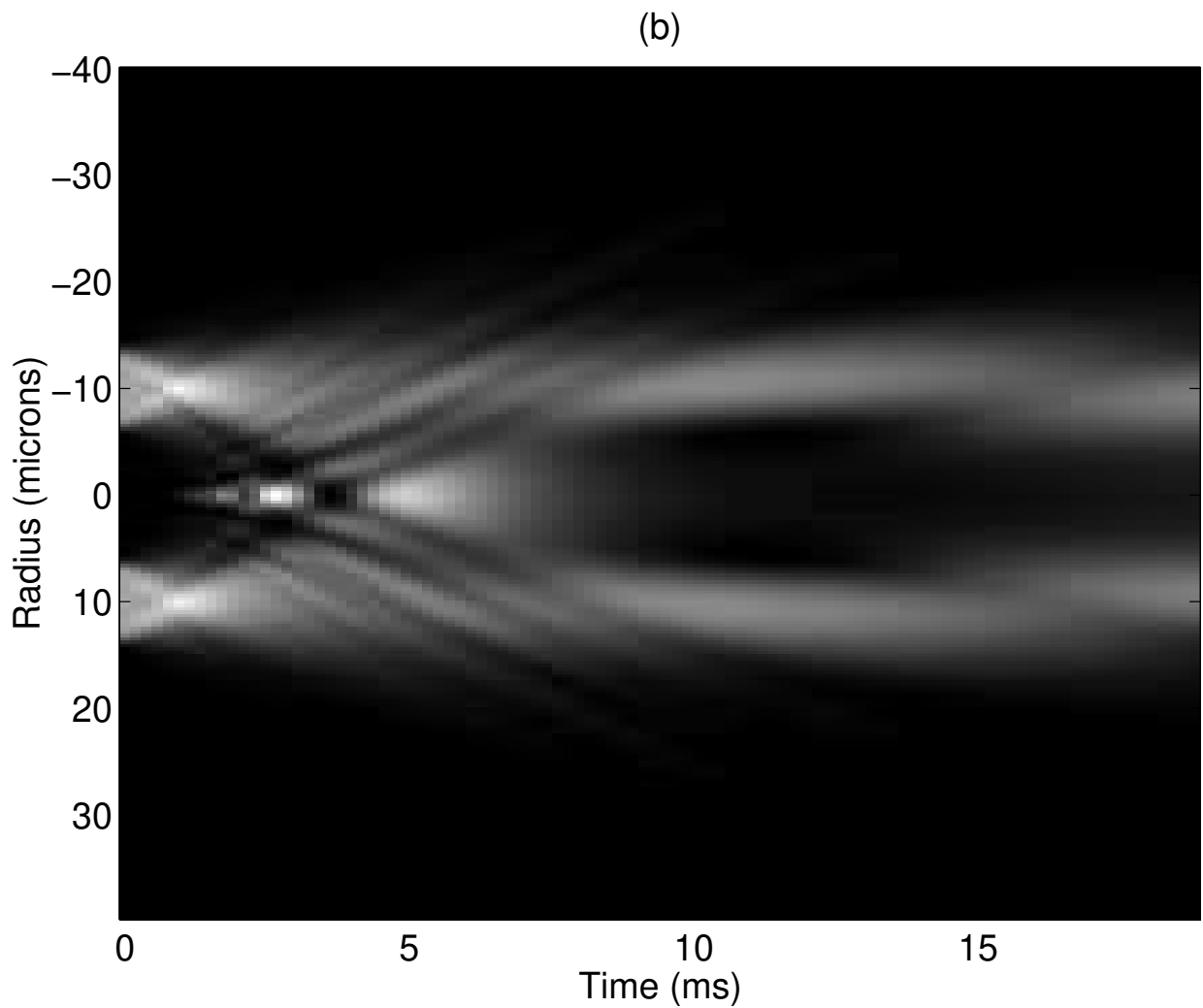


Figure 4(b)

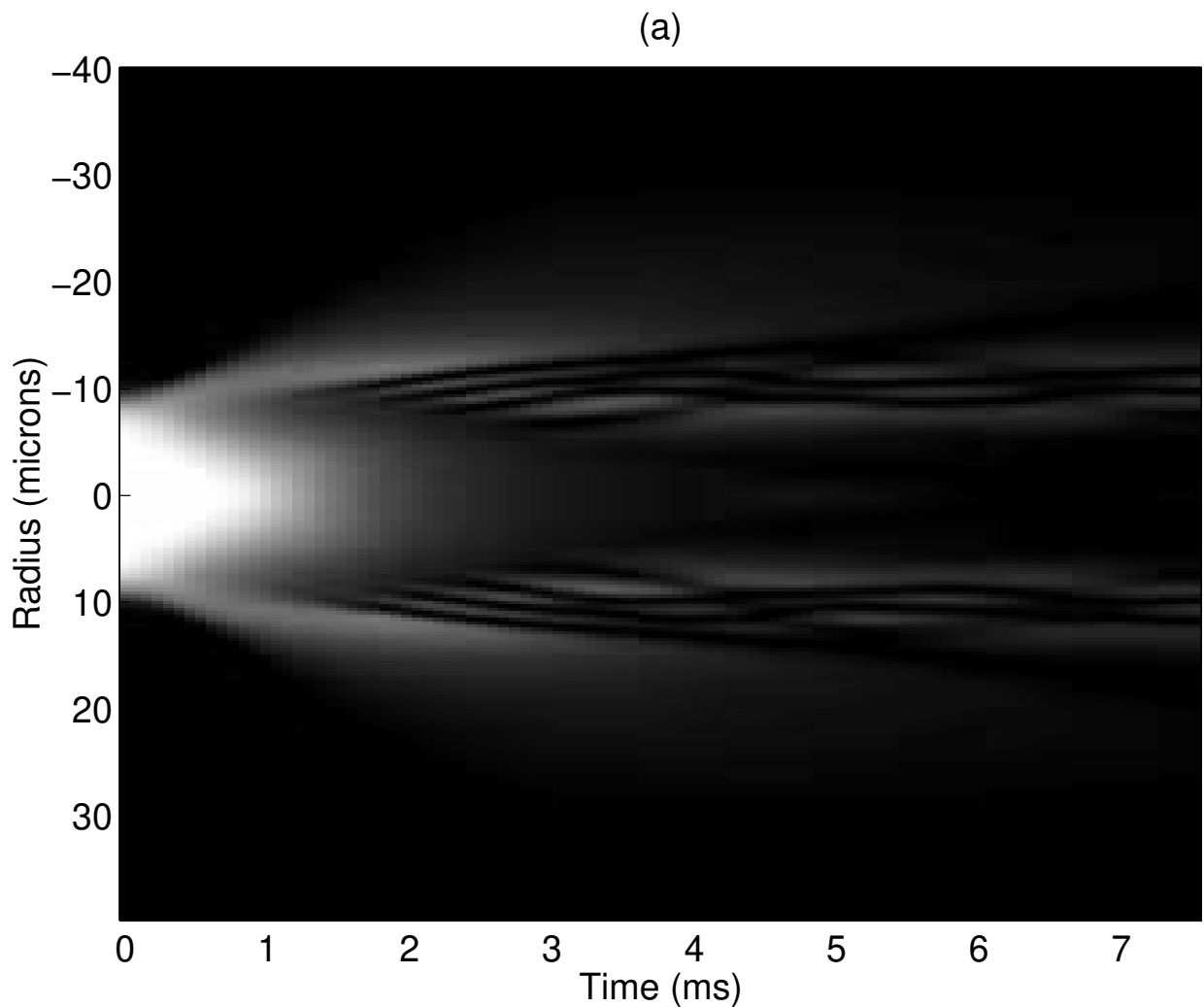


Figure 5(a)

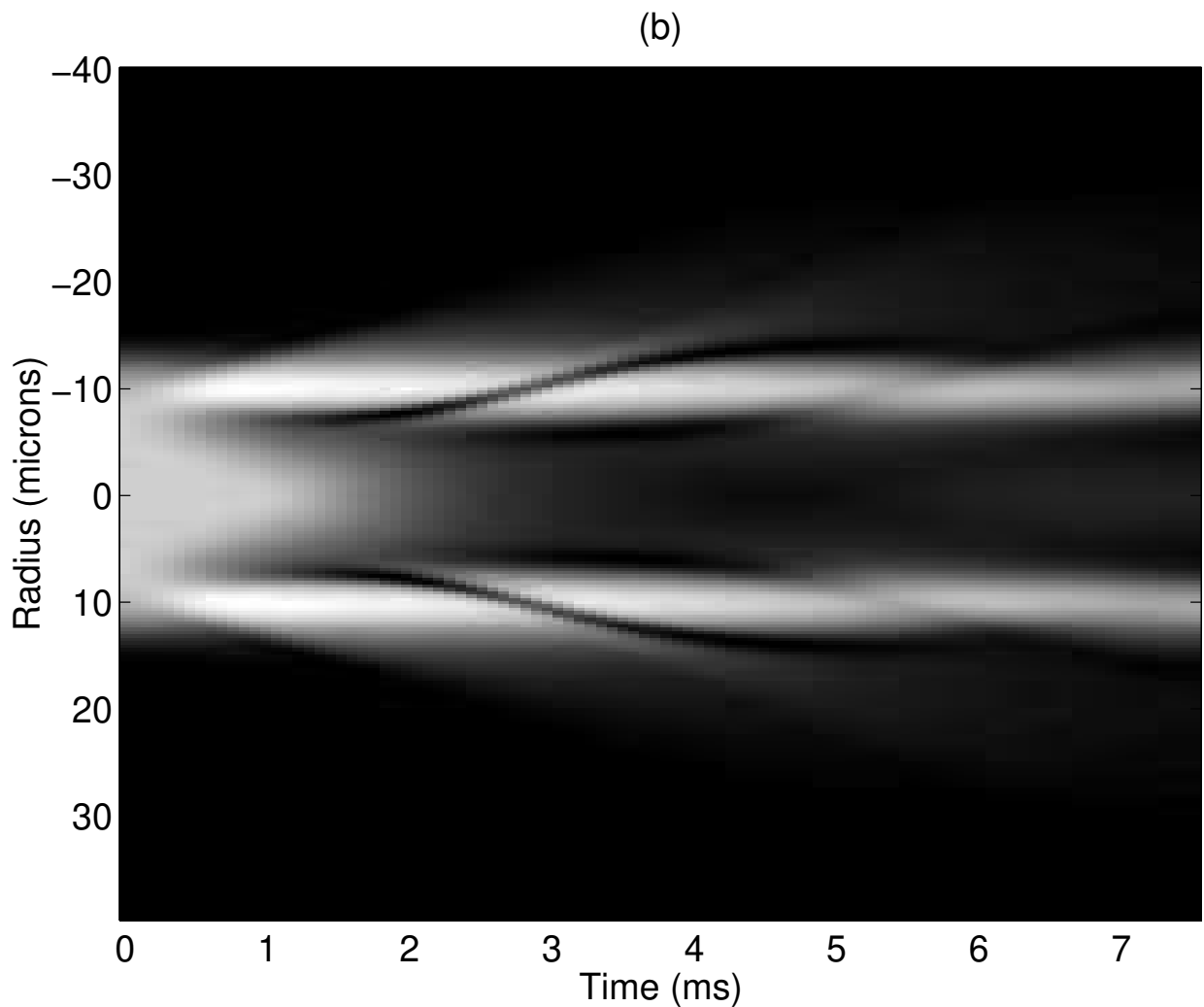


Figure 5(b)

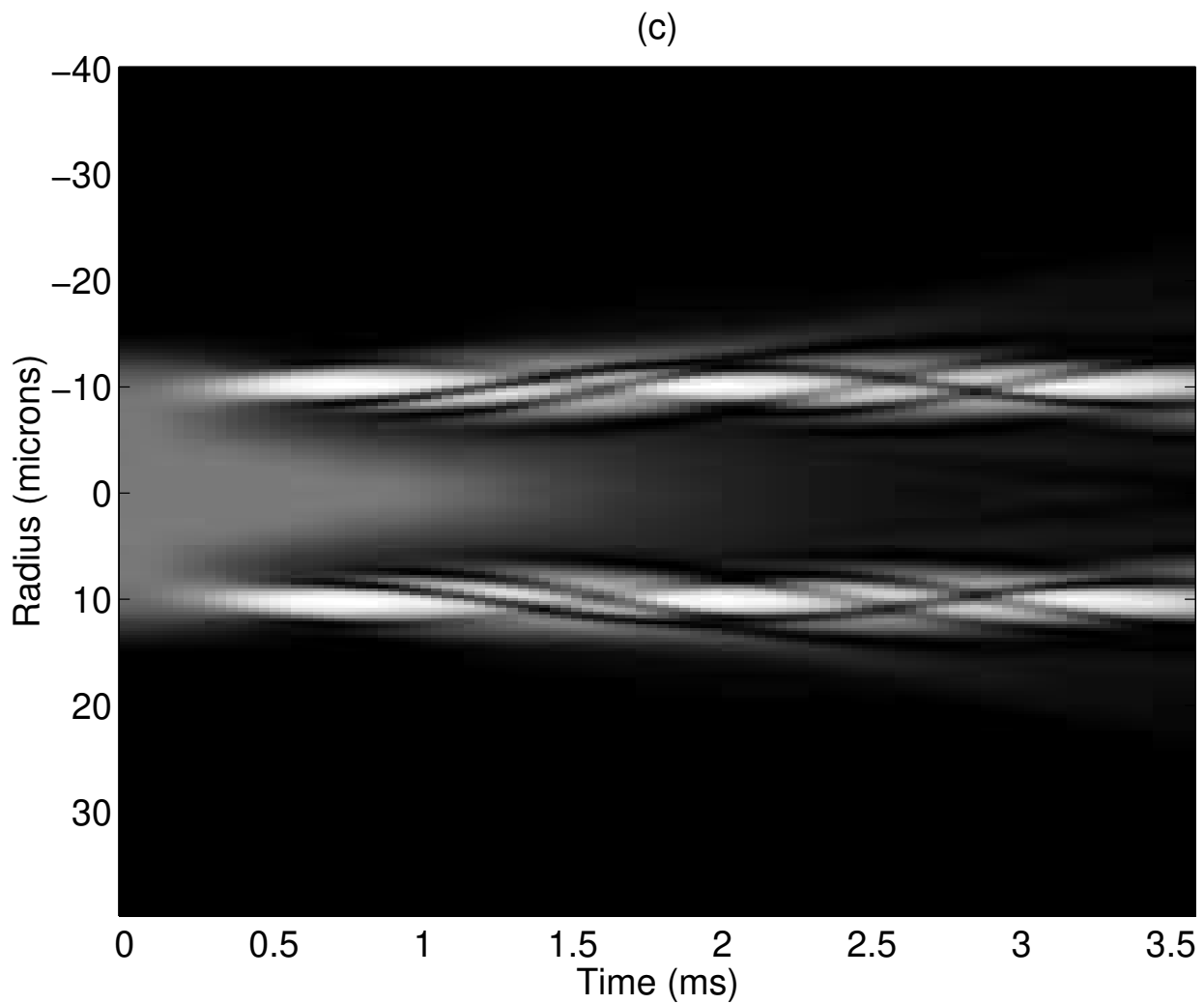


Figure 5(c)